Biomimetic and Biofeedback approaches for Brain Machine Interface

Biomimetic and Biofeedback approaches for Brain Machine Interface

Kianoush Nazarpour and Andrew Jackson
Institute of Neuroscience, Newcastle University, Newcastle-upon-Tyne NE2 4HH, UK
E-mails: {K.Nazarpour, Andrew.Jackson}@ncl.ac.uk

***Abstract*—In this paper, we elaborate on the distinction between classic approaches towards brain machine interface (BMI), that is Biomimetic and Biofeedback, and discuss their advantages and disadvantages. For biomimetic BMI, we briefly report results of a novel constrained Kalman filtering-optimization mechanism for prediction of myoelectric signals from neural spike recordings in a behaving macaque monkey. For the Biofeedback BMI, we review early works on operant conditioning and our recent results on emulating BMI by a myoelectric control interface.**

I. Introduction

Biomimetic brain-machine interfaces (BMI) have evolved from experimental paradigms which explore neural coding of natural arm and hand movements to current real-time neural firing rates decoders in humans or behaving monkeys [1], [2], [3]. In a typical BMI setup, monkeys perform stereotyped repeated arm or hand movements, e.g. the classic center-out task or random target tracking using a manipulandum, and the firing rates of tens of individual motor cortex neurons are fitted to arm kinematics, (e.g. position and velocity). The estimated mapping is then used to drive an artificial effector. While neural activity recorded from primary motor (M1) cortex is well documented to have high correlations with kinetic parameters of movement as well as kinematics [4], [5], [6], relatively few studies have addressed the kinetic component (for exceptions, see [7]).

Despite recent decoding algorithms with increasing level of sophistication, BMI control remains slow and inaccurate in comparison to natural movements. Therefore, considerable improvements are required if these devices are to have real-life clinical applications. The main question to be answered here is whether developing more sophisticated algorithms for trajectory decoding (Biomimetic) would be more useful for future real-life BMI applications or devising new BMI control environments which exploit the brain's inherent flexibility to tune control parameters through biofeedback.

However, current multi-electrode and multi-site recording techniques enable the simultaneous registration of neural spiking activity from tens to hundreds of neurons so that a decoder might make use of the underlying functional connectivity between the neurons, together with the individual rate codes [8]. In [7] several approaches for biomimetic BMI including simple linear neural activity decoders and ambitious closed-loop BMI by stimulating the sensory cortex [to restore the loss of sensation] are listed. In general in biomimetic BMI, firing rate of motor cortex neurons are fitted to arm trajectory kinematics. Although these fitting algorithms are mathematically impressive and provide acceptable performance, they suffer from poor generalization and therefore, clumsy real-time control when compared to natural arm movements. The main problem, we think, is the absence of any fast error correction mechanism as all of the movement corrections are mediated by visual feedback. Fagg et al. in [7] argue that lack of proprioception is a considerable shortcoming of the classic biomimetic and suggests stimulation sensory cortex to restore it. The importance of proprioceptive feedback is challenged in [9].

1) Biomimetic BMI: We have recently developed a point process-generalized linear model (GLM) that accommodates the neuron's own spiking history, concurrent ensemble activity, and extrinsic covariates such as visual stimuli or behavioral measures to estimate a given in the neuron's spiking probability [10], [11]. Several variations of such an adaptive point process filter or its Gaussian counterpart, the classic Kalman filter, have appeared in the literature which reliably decode arm movement kinematics [12], [13]. Nevertheless, a fundamental limitation in using filters from the Kalman family for prediction is their sub-optimality in dealing with non-Gaussian observations or systems in which the state evolution violates the linear-Gaussian Markov process assumption. Here, we report an alternative approach for electromyogram (EMG) prediction from multi-channel neural spike recordings in the state-space recently introduced in [14]. Unlike the conventional Kalman filtering based motor decoders in the BMI literature, we employ a GLM similar to that proposed in [11].

2) Biofeedback BMI: In this approach once a few operational rules have been acquired, control of the interface is optimised by the user through reinforcement or error-based learning [15], [16], [17], [18]. The decoder is usually very simple and fixed. For instance, linear combinations of a few neurons control the position of a cursor on a screen. Biofeedback BMI provides the exciting possibility to study the neural correlates of motor learning within the BMI framework [18], [19].

This paper is organized as follows. Section II very briefly describes the constrained Kalman filtering method and reports the results. The interested reader may refer to [14] for further details. In Section III, we will review classic [15], [16] and recent [17], [18] suggestions for biofeedback BMI and report our earlier results [9], [19]. Section IV, concludes the paper.

Proceedings of the Second APSIPA Annual Summit and Conference, pages 207–211,
Biopolis, Singapore, 14-17 December 2010.

II. BIOMIMETIC BMI: EMG PREDICTION IN STATE-SPACE [14]

In the classic Kalman filter setting, the hidden state and observation vectors at time k are respectively denoted by $\mathbf{q}_k$ and $\mathbf{y}_k$ and both evolve as Markov processes completely defined by $p(\mathbf{q}_{k+1}|\mathbf{q}_k)$ and $p(\mathbf{y}_k|\mathbf{q}_k)$. Therefore, $\mathbf{q}_{k+1}|\mathbf{q}_k \sim \mathcal{N}(\mathbf{q}_k; \mathbf{A}\mathbf{q}_k, \mathbf{C}_\mathbf{q})$ and $\mathbf{y}_k|\mathbf{q}_k \sim \mathcal{N}(\mathbf{y}_k; \mathbf{B}\mathbf{q}_k, \mathbf{C}_\mathbf{y})$ where $\mathcal{N}(\mathbf{a}; \boldsymbol{\mu}, \mathbf{C})$ denotes $\mathbf{a}$ is a Gaussian distributed vector with mean vector $E[\mathbf{a}] = \boldsymbol{\mu}$ and covariance matrix $\mathbf{C}$. The system parameters, $\mathbf{A}, \mathbf{B}, \mathbf{C}_\mathbf{q}$, and $\mathbf{C}_\mathbf{y}$ are assumed to be fixed.

Several different instantiation of this recursive Gaussian approximation have been introduced. However, in order to circumvent the above shortcomings, all have places the neural and behavioral data into bins of greater than 70 ms duration [12], [13], [20]. This approach has been effective for prediction of the kinematics of arm movements where arm positions and directional velocities can be modeled as Markov linear-Gaussian processes [21]. However, the Kalman setting is not effective in prediction of EMG signals, the dynamics of which, $p(\mathbf{q}_k|\mathbf{q}_{k-1})$, are not smooth. The power in an EMG signals is typically computed following rectification, in order to extract the modulation envelope. This constrains the state variable $\mathbf{q}_k$ to be non-negative, leading to a discontinuity in $\log p(\mathbf{q}_k|\mathbf{q}_{k-1})$ at $\mathbf{q}_k = 0$. The forward distribution $p(\mathbf{q}_k|\mathbf{y}_{1:k})$ turns out to be non-Gaussian. The breakdown of the basic Kalman assumptions is inevitable, as there is no mechanism to constrain the estimates to be non-negative.

Direct Optimization Interpretation of Kalman Filters: The objective in using a Kalman filter is to compute the conditional expectation of the hidden state path $\mathbf{q}_{1:K}$ given the observations $\mathbf{y}_{1:K}$, that is $E(\mathbf{q}_{1:K}|\mathbf{y}_{1:K})$. In a linear-Gaussian setting, $(\mathbf{q}_{1:K}, \mathbf{y}_{1:K})$ forms a jointly Gaussian random variable, and therefore $p(\mathbf{q}_{1:K}|\mathbf{y}_{1:K})$ remains Gaussian. Coincidence of the mean and mode of a Gaussian distribution implies that $E(\mathbf{q}_{1:K}|\mathbf{y}_{1:K})$ is in fact equal to the maximum a posteriori (MAP) solution, i.e., the maximizer of the posterior $p(\mathbf{q}_{1:K}|\mathbf{y}_{1:K})$. Reformulating the Kalman filter in an optimization framework leads to equations (1) and (2). Notice that $\mathbf{Q}$ forms a quadratic function of $\mathbf{q}_{1:K}$

$$\begin{aligned}\mathbf{Q} &= \arg\max_{\mathbf{q}_{1:K}} p(\mathbf{q}_{1:K}|\mathbf{y}_{1:K}) = \arg\max_{\mathbf{q}_{1:K}} \Bigg(\log p(\mathbf{q}_1) \\ &+ \sum_{k=2}^{K} \log p(\mathbf{q}_k|\mathbf{q}_{k-1}) + \sum_{k=1}^{K} \log p(\mathbf{y}_k|\mathbf{q}_k) \Bigg) \end{aligned} \quad (1)$$

Therefore,

$$\begin{aligned}\mathbf{Q} &= \arg\max_{\mathbf{q}_{1:K}} \Bigg[-\frac{1}{2} \Bigg((\mathbf{q}_1 - E(\mathbf{q}_1))^T \mathbf{C}_{\mathbf{q}_1}^{-1} (\mathbf{q}_1 - E(\mathbf{q}_1)) \\ &+ \sum_{k=2}^{K} (\mathbf{q}_k - \mathbf{A}\mathbf{q}_{k-1})^T \mathbf{C}_\mathbf{q}^{-1} (\mathbf{q}_k - \mathbf{A}\mathbf{q}_{k-1}) \\ &+ \sum_{k=1}^{K} (\mathbf{y}_k - \mathbf{B}\mathbf{q}_k)^T {\mathbf{C}_\mathbf{y}}^{-1} (\mathbf{q}_k - \mathbf{B}\mathbf{q}_k) \Bigg) \Bigg]. \end{aligned} \quad (2)$$

The quadratic form $\mathbf{Q}$ implies that it may be solved by an unconstrained quadratic program in $\mathbf{q}_{1:K}$ as in [22], [23]. Therefore,

$$\begin{aligned}\hat{\mathbf{q}}_{1:K} &= \arg\max_{\mathbf{q}_{1:K}} \log p(\mathbf{q}_{1:K}, \mathbf{y}_{1:K}) \\ &= \arg\max_{\mathbf{q}_{1:K}} \left[\frac{1}{2} \mathbf{q}_{1:K}^T \mathbf{H} \mathbf{q}_{1:K} + \boldsymbol{\nabla}^T \mathbf{q}_{1:K} \right] = -\mathbf{H}^{-1} \boldsymbol{\nabla} \end{aligned} \quad (3)$$

where Hessian $\mathbf{H}$ and gradient $\boldsymbol{\nabla}$ of $\log p(\mathbf{q}_{1:K}|\mathbf{y}_{1:K})$ are computed as

$$\boldsymbol{\nabla} = \boldsymbol{\nabla}_{\mathbf{q}_{1:K}} p(\mathbf{q}_{1:K}|\mathbf{y}_{1:K})|_{\mathbf{q}_{1:K}=\mathbf{0}} \quad (4)$$

$$\mathbf{H} = \boldsymbol{\nabla}\boldsymbol{\nabla}_{\mathbf{q}_{1:K}} p(\mathbf{q}_{1:K}|\mathbf{y}_{1:K})|_{\mathbf{q}_{1:K}=\mathbf{0}}; \quad (5)$$

the Hessian $\mathbf{H}$ of $\log p(\mathbf{q}_{1:K}|\mathbf{y}_{1:K})$ is a block-tridiagonal matrix and its elements may be readily computed [14].

So far, we have assumed that $p(\mathbf{y}_k|\mathbf{q}_k)$ is Gaussian distributed. However, spike recordings are point processes sampled from the poisson distribution. It is straightforward to extend the above optimization approach to directly compute MAP estimate of $\mathbf{q}_{1:K}$ in a general non-Gaussian case.

Here, we assume that, $\log p(\mathbf{q}_{k+1}|\mathbf{q}_k)$ is a concave function of $\mathbf{q}_{1:K}$ and that the initial density $\log p(\mathbf{q}_0)$ is concave and also that the observation density $\log p(\mathbf{y}_k|\mathbf{q}_k)$ is concave in $\mathbf{q}_k$ [24]. Then, it is easy to show that the log-posterior $\log p(\mathbf{q}_{1:K}|\mathbf{y}_{1:K})$ is concave and hence the MAP estimation of $\mathbf{q}_{1:K}$ is a concave problem. The standard Newton's algorithm can be applied to optimize such an estimate as $\hat{\mathbf{q}}_{1:K}^{i+1} = \hat{\mathbf{q}}_{1:K}^{i} - \mathbf{H}^{-1}\boldsymbol{\nabla}$.

$p(\mathbf{y}_k|\mathbf{q}_k)$ represents the probability of neural firings given an external covariate, a sensory stimulus or a motor output. It has been shown in [10], among others, that the conditional intensity function $\lambda_k(h_k)$ can fully characterize the stochastic neural point process as

$$\lambda_k(h_k) = \lim_{\kappa \to 0} \frac{p(N(k+\kappa) - N(k) = 1|h_k)}{\kappa} \quad (6)$$

where $p(N(k+\kappa))$ is a conditional probability, h_k incorporates the spiking history up to time k, and $\lambda_k(h_k)$ is a strictly positive function [10]. For small κ, $\lambda_k(h_k)$ attains approximately the neuron's spiking probability in the time interval $\Delta t_k = (k, k+\kappa]$. In the GLM setting, h_k pertains the neuron's own spiking history and the extrinsic covariates.

Therefore, as in [10], for an ensemble of C neurons we have

$$\log p(\mathbf{y}_k|\mathbf{q}_k) = \sum_{i=1}^{C} \Big((\lambda_k^i \triangle t_k)^{\triangle N_k^i} \exp(\lambda_k^i \triangle t_k) \Big). \quad (7)$$

Mean firing rate for neuron i at time k, denoted by λ_k^i, is estimated by a GLM that accounts for the neuron's base firing rate and a linear regression from the extrinsic covariate to individual neurons passed through an exponential non-linearity. This GLM setting is hence of the form $\lambda_k^i = f\big(\mathfrak{b}_i + \mathfrak{B}_i^T \mathbf{q}_k\big)$ where $f(.)$ is a convex and log-concave function, $\mathfrak{b}_i$ is a constant offset term representing the baseline firing rate of

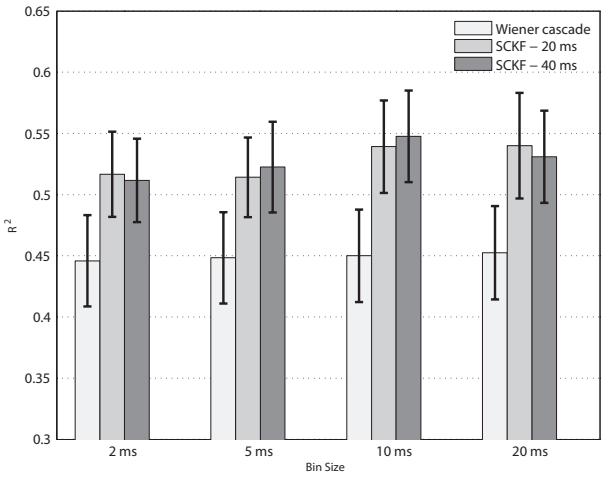

Fig. 1. Summary of EMG prediction generalization accuracy using SCKF (20 ms and 40 ms time delay) and Wiener cascade filter in four different bin sizes. The average R^2 values and their associated standard error of means were found by 20-fold cross-validations. Generalizations accounted for 50-55% of the the actual EMGs for the SCKF which was higher than that of the Wiener cascade filter by 5-10%. The prediction accuracy of the SCKF slightly improves by larger bin sizes but the delay between spikes and EMGs does not much influence the generalization.

i-th neuron and the i-th row $\mathfrak{B}_i$ of the observation matrix $\mathfrak{B}$ encapsulates the i-th neuron's preference for target muscles. The log-concavity of $f(.) \equiv \exp(.)$ allows us to use the standard Gaussian approximation of the forward non-Gaussian probabilities $p(\mathbf{q}_k, \mathbf{y}_{1:k})$.

Log-Barrier Method for Constrained Optimization: The strictly positive envelope of rectified EMGs is predicted drives the BMI [25]. Therefore, for EMG prediction we may not utilize the above representations of the Kalman filter unless a constrained optimization problem be formed. To handle this constraint problem, the standard interior-point (log-barrier) methods [22], [23], [24] is employed by replacing the constrained concave problem

$$\hat{\mathbf{q}}_{1:K}^{MAP} = \arg \max_{\mathbf{q}_{1:K}:\mathbf{q}_k>0} \log p(\mathbf{q}_{1:K}|\mathbf{y}_{1:K}) \tag{8}$$

with a sequence of unconstrained concave problems

$$\hat{\mathbf{q}}_{1:K}^{\epsilon} = \arg \max_{\mathbf{q}_{1:K}} \log p(\mathbf{q}_{1:K}|\mathbf{y}_{1:K}) + \epsilon \sum_k \log \mathbf{q}_k. \tag{9}$$

Incorporating the penalty term enforces $\hat{\mathbf{q}}_{1:K}^{\epsilon}$ to satisfy the non-negativity constraint, for $\log u \to -\infty$ as $u \to 0$. It is easy to show that if $\hat{\mathbf{q}}_{1:K}^{MAP}$ is unique, then $\hat{\mathbf{q}}_{1:K}^{\epsilon}$ converges to $\hat{\mathbf{q}}_{1:K}^{MAP}$ as $\epsilon \to 0$.

Data Acquisition and Results: The experiment involved one rhesus macaque monkey, chronically implanted with a multi-electrode array (Blackrock Microsystems Inc., Utah) in the arm area of motor cortex. Details of the surgical procedure have been described previously in [26]. Neural data was collected, at 25 KHz sampling rate, using a 96-channel Cerebus acquisition system (Blackrock Microsystems Inc., Utah). The monkey was also implanted with chronic intramuscular EMG electrodes in twelve forearm and hand muscles routed subcutaneously to a percutaneous connector. The EMG activity from all muscles was sampled at a rate of 2 KHz.

The monkey's behavioral task consisted of applying a grip force to a ball to control the vertical movement of a small circular cursor on a screen. The monkey placed its hand on a touch pad to start each trial, until receiving a "Go" tone. The ball, which was held by the experimenter in front of the monkey, was connected by a flexible tube to a pressure transducer which provided an estimate of grip force. The monkey was allowed five seconds after the "Go" tone to reach for and squeeze the ball, and then was required to hold the cursor inside a target for 0.8 seconds. Following successful trials, the monkey received a controlled amount of fruit juice. We conducted two experiments in three days. In the first two days, after a short (5-10 minute) *warm up* period, we recorded three, six-minute data files. Single and multi-unit spike signals were sorted on the first day, using 2D PCA-space visualization computed with the Cerebus software. This sorting was kept constant in the second day. Discriminated time stamps were further analyzed in Matlab. Following [26], the EMG envelopes in each channel were extracted by highpass filtering at 50 Hz, rectification, and lowpass filtering at 10 Hz. During the task, the neural data and the EMG activity were recorded simultaneously along with task relevant sensor signals, e.g. pressure. Both spike recordings and EMG signals were downsampled to various bin sizes (2, 5, 10, and 20 ms) for further analysis.

20 fold cross-validated results are reported, in which 19 folds were used for training the model and one fold for testing. Mean prediction rates are presented in terms of the coefficient of determination R^2 and either standard deviation. We compared the results with the results of the conventional Wiener cascade filters. Briefly, in the Wiener filtering approach, the EMG activity are predicted using a linear system with multiple inputs and a single output. In such a filter, each neural input is convolved with its causal finite impulse response function to produce a single output. The length of this filter is typically 250 ms. This linear system can be followed by a static non-linearity to form the Wiener cascade model. Hence, the output of such a system is a linear, weighted combination of the recent history of neural signals, transformed by a second or third order polynomial, that is the static non-linearity. In practice, the non-linearity acted both as a threshold that eliminated small signal fluctuations in the predictions when muscles were quiescent, and to amplify the estimated peaks EMG activity [27], [26].

Figure 1 reports a summary of EMG prediction generalization accuracy in four different bin size. Generalization predictions made by the SCKF[1] reasonably accounted up to 55% of the actual EMGs. In comparison to the rates obtained by the Wiener cascade filter, 5-10% improvement

[1]SCKF stands for simplified constrained Kalman filter. [14] reports the results of fully constrained Kalman filter in which the GLM model includes the terms corresponding to the interactions between cells and firing history of each cell.

was achieved. A slight improvement in prediction rates was observed using larger bin sizes by the Kalman filter, in contrast to Wiener cascade filter. The delay between spikes and EMGs did not influence the generalization capacity for SCKF.

III. Biofeedback BMI: A Short Review

The traditional biomimetic BMI paradigm has its historical roots in experimental studies elucidating the neural correlates of natural movements. Neural activity is recorded in animals performing a trained motor task to determine how the firing rate of cortical neurons is related to (or "encodes" particular movement parameters [28], [29], [30]. The biomimetic BMI approach inverts these relationships between cells and movements in order to "decode" motor output.

By contrast, the biofeedback BMI approach is motivated by experimental demonstrations that the relationship between cell activity and behaviour can be altered through operant conditioning. In these experiments, animals were rewarded for producing arbitrary combinations of cell and/or muscle activity [15], [31] and rapidly learned to dissociate their normal neuromotor patterns. This suggests that there is considerable flexibility to neural "encoding" which may enable learning novel neuromotor associations [9]. These findings are important since it is unlikely that a biomimetic BMI will ever be able to exactly match the complex efferent and afferent connections of the limb it is replacing. Therefore exploiting the brain's plasticity and ability to learn new motor tasks will be an important component of successful BMI applications.

Moritz *et al.* in [17], building upon early studies in [15], [16] showed that monkeys can control functional electrical stimulation (FES) of muscles using M1 neuronal activity to restore movements in a temporarily paralyzed arm. In their system, the animal was trained to modulate a smoothed cell firing rate to control proportional muscle stimulation such that if the activity exceeded a threshold the stimulator was switched on and the wrist was extended. Interestingly they found that after training, the quality of control achieved with individual cells was unrelated to that cell's tuning strength during normal wrist movements. They further developed this approach to control both wrist flexion and extension when the firing rate of one single cell falls out of a defined frequency band, and succeeded in conditioning pairs of neurons to collaboratively control the FES.

In a recent study [18], Ganguly and Carmena used a 2-D BMI decoder in which the directions that neurons act on the cursor are randomised. Importantly they used only a subset of recorded cells which showed stable activity over a period of up to 20 days. This afforded the animal time to practise over several days and consolidate a stable neural representation of the BMI. Interestingly, the animal was then able to learn a new random decoder based on the same set of neurons, and readily switch between the two when required.

We are interested in the mechanisms by which the brain learns these abstract, non-intuitive neuromotor transformations. To explore this question with non-invasive techniques in human subjects we use a myoelectric-controlled interface (MCI). Rectified and smoothed EMG activity from multiple hand and arm muscles is mapped onto a 2-D cursor space through a linear combination of vectors aligned to a direction of action (DoA). In our first study [9] we compared "intuitive" control, in which muscles acted on the cursor in directions that were consistent with their action on the hand given the subject's posture, with "nonintuitive" control when muscle DoAs were randomly assigned. Although performance was initially poorer under nonintuitive arrangements, with practice subjects learned to make direct, feed-forward movements towards the target. Within about 30 minutes performance plateaus at a high level that is comparable to control under the intuitive mapping.

We then tested the importance of proprioceptive feedback from muscles by introducing random sensory noise through vibration, but this did not affect the rate at which learning progressed. We suggest that acquiring MCI control involves learning the association between an internal copy of the efferent motor command and the visual feedback from the cursor. The apparent ease with which subjects could learn this association is in contrast to the longer time-frame required to acquire a randomised BMI decoder in animal studies [18]. Nevertheless, the results of Ganguly and Carmena suggest that given sufficient time, the brain can learn novel efference-feedback mappings at the neural level. If so, then utilizing these mechanisms may potentially be more effective than accurate biomimetic decoding.

IV. Conclusions

In this paper we briefly compared the classic biomimetic and biofeedback approaches to BMI. For biomimetic BMI we reported results of novel signal processing method to predict muscle activity from neural recording and for biofeedback, we briefly reviewed classic work on operant conditioning and its relevance to recent BMI and MCI studies.

The accuracy of BMI decoding algorithms has yet to be improved before existing proof-of-principle demonstrations can be translated into viable clinical applications. After decades of BMI research, it seems appropriate to reassess the current approaches to BMI and explore alternatives to address the shortcoming of existing protocols. For instance, it has been established that in order to make accurate reaching movements, the human motor system employs an optimal combination of feed-forward prediction and visual/proprioceptive feedback [32]. In biomimetic designs, the decoded trajectories are corrected only via visual feedback, leading to jerky movements. In other words, BMI control may seem more like concatenation of several feed-forward movement segments rather than the smooth operation of a closed-loop feedback controller. Similar clinical observations have been described in deafferented patients suffering from loss of proprioception [33]. However, motor errors during natural movements may reflect uncertainty about the state (kinematics and kinetics) of the limb and the external world. In the BMI setting, the movement of the cursor is an entirely predictable consequence of the efferent signal. Therefore, trajectory errors likely reflect central noise

in the motor system, which is exacerbated since only a small proportion of neurons within motor cortex are sampled. The mechanisms by which the brain deals with variability in neural firing patterns during natural movements [34] are only now beginning to be understood [19], [35] but these insights have yet to be developed within a BMI setting.

Although we have here contrasted biomimetic and biofeedback approaches, the ultimate success of BMI applications will likely to require some combination of both. Current biofeedback experiments may be improved by incorporating the sophisticated decoding algorithms already matured in the biomimetic setting. In turn, insights about the mechanisms of neural adaptation from biofeedback experiments may be incorporated into new adaptive biomimetic decoders, Hopefully, such best of both strategies will lead to a new generation of machines that interface with the brain on computational, algorithmic and implementational levels, according to Marr's Tri-Level Hypothesis [36], to restore sophisticated function following injury.

ACKNOWLEDGMENT

This works is supported in parts by The Wellcome Trust, Medical Research Council, UK, and Newcastle University. We acknowledge contribution of Prof L Miller at Northwestern University and Dr L Paninski at Columbia University in developing and implementing the constrained Kalman filter presented in Section II.

REFERENCES

[1] A. B. Schwartz, "Direct cortical representation of drawing," *Science*, pp. 540–542, 1994.

[2] M. D. Serruya, N. G. Hatsopoulos, L. Paninski, M. R. Fellows, and J. P. Donoghue, "Instant neural control of a movement signal," *Nature*, p. 141142, 2008.

[3] J. Wessberg, C. R. Stambaugh, J. D. Kralik, P. D. Beck, M. Laubach, J. K. Chapin, J. Kim, S. J. Biggs, M. A. Srinivasan, and M. A. Nicolelis, "Real-time prediction of hand trajectory by ensembles of cortical neurons in primates," *Nature*, pp. 361–365, 2000.

[4] A. P. Georgopoulos, J. Ashe, N. Smyrnis, and M. Taira, "The motor cortex and the coding of force," *Science*, pp. 1692–1695, 1992.

[5] E. V. Evarts, "Relation of pyramidal tract activity to force exerted during voluntary movement," *J. Neurophysiol.*, pp. 14–27, 1968.

[6] M. M. Morrow, L. R. Jordan, and L. E. Miller, "Direct comparison of the task-dependent discharge of m1 in hand space and muscle space," *J. Neurophysiol.*, pp. 1786–1798, 2007.

[7] A. H. Fagg, N. G. Hatsopoulos, V. de Lafuente, K. A. Moxon, S. Nemati, J. M. Rebesco, R. Romo, S. A. Solla, J. Reimer, D. Tkach, E. A. Pohlmeyer, and L. E. Miller, "Biomimetic brain machine interfaces for the control of movement," *J. Neurosci*, vol. 27, no. 44, pp. 11842–11846, 2007.

[8] I. H. Stevenson, J. M. Rebesco, L. E. Miller, and K. P. Körding, "Inferring functional connections between neurons," *Curr. Opin. NeuroBiol.*, pp. 582–588, 2008.

[9] S. M. Radhakrishnan, S. N. Baker, and A. Jackson, "Learning a novel myoelectric-controlled interface task," *J Neurophysiol.*, vol. 100, no. 4, pp. 2397–2408, 2008.

[10] W. Truccolo, U. T. Eden, M. R. Fellows, J. P. Donoghue, and E. N. Brown, "A point process framework for relating neural spiking activity to spiking history, neural ensemble, and extrinsic covariate effects," *J. Neurophysiol*, vol. 93, pp. 1074–1089, 2005.

[11] J. Pillow, J. Shlens, L. Paninski, A. Sher, A. Litke, E. Chichilnisky, and E. Simoncelli, "Spatiotemporal correlations and visual signaling in a complete neuronal population," *Nature*, vol. 454, pp. 995–999, 2008.

[12] W. Wu, Y. Gao, E. Bienestock, J. P. Donoghue, and M. J. Black, "Bayesian papulation decoding of motor cortical activity using a Kalman filter," *Neural Computation*, vol. 18, no. 1, pp. 80–118, 2006.

[13] W. Wu, J. E. Kulkarni, N. G. Hatsopoulos, and L. Paninski, "Neural decoding of hand motion using a linear state-space model with hidden states," *IEEE Trans. Neural Syst. Rehabil. Eng.*, vol. 17, no. 4, pp. 370–378, 2009.

[14] K. Nazarpour, C. Ethier, L. Paninski, J. M. Rebesco, R. C. Miall, and L. E. Miller, "EMG prediction from motor cortical recordings in the state-space," in preparation.

[15] E. E. Fetz and D. V. Finocchio, "Correlations between activity of motor cortex cells and arm muscles during operantly conditioned response patterns," *Exp. Brain Res.*, vol. 23, no. 3, pp. 217–240, 1975.

[16] E. E. Fetz and R. I. Barensten, "An electronic activity integrator for operant conditioning of patterns of neural and muscular activity," *Electroencephalogr. Clin. Neurophysiol.*, vol. 38, no. 1, pp. 87–90, 1975.

[17] C. T. Moritz, S. I. P. SI, and E. E. Fetz, "Direct control of paralysed muscles by cortical neurons," *Nature*, vol. 456, no. 7222, pp. 639–42, 2008.

[18] K. Ganguly and J. M. Carmena, "Emergence of a stable cortical map for neuroprosthetic control," *PLoS Biol.*, vol. 7, no. 7, p. e1000153, 2009.

[19] K. Nazarpour and A. Jackson, "Flexible cortical control of task-specific muscle synergies," in *SfN*, 2010.

[20] A. E. Brockwell, A. L. Rojas, and R. E. Kass, "Recursive bayesian decoding of motor cortical signals by particle filtering," *J. Neurophysiol.*, p. 18991907, 2004.

[21] B. M. Yu, C. Kemere, G. Santhanam, A. Afshar, S. I. Ryu, T. H. Meng, M. Sahani, and K. V. Shenoy, "Mixture of trajectory models for neural decoding of goal-directed movements," *J. Neurophysiol.*, p. 37633780, 2007.

[22] L. Paninski, Y. Ahmadian, D. G. Ferreira, S. Koyama, K. Rahnama Rad, M. Vidne, J. Vogelstein, and W. Wu, "A new look at state-space models for neural data," *J. Comput. Neuroscience*, 2009. DOI 10.1007/s10827-009-0179-x.

[23] S. Boyd and L. Vandenberghe, *Convex Optimization*. Oxford University Press, 2004.

[24] S. Koyama and L. Paninski, "Efficient computation of the maximum a posteriori path and parameter estimation in integrate-and-fire and more general state-space models," *J. Comput. Neuroscience*, 2009. DOI 10.1007/s10827-009-0150-x.

[25] E. A. Pohlmeyer, E. R. Oby, E. J. Perreault, S. A. Solla, K. L. Kilgore, R. F. Kirsch, and L. E. Miller, "Toward the restoration of hand use to a paralyzed monkey: Brain-controlled functional electrical stimulation of forearm muscles," *PLoS ONE*, vol. 4, pp. 1–8, 2009.

[26] E. A. Pohlmeyer, S. A. Solla, E. J. Perreault, and L. E. Miller, "Prediction of upper limb muscle activity from motor cortical discharge during reaching," *J. Neural Eng.*, vol. 4, pp. 369–379, 2007.

[27] D. T. Westwick, E. A. Pohlmeyer, S. A. Solla, L. E. Miller, and E. J. Perreault, "Identification of multiple-input systems with highly coupled inputs: application to EMG prediction from multiple intracortical electrodes," *Neural Computation*, vol. 18, no. 2, pp. 329–355, 2006.

[28] A. Georgopoulos, J. Kalaska, R. Caminiti, and J. Massey, "On the relations between the direction of two-dimensional arm movements and cell discharge in primate motor cortex," *J. Neurosci*, vol. 2, p. 15271537, 1982.

[29] E. V. Evarts, "Pyramidal tract activity associated with a conditioned hand movement in the monkey," *J. Neurophysiol.*, pp. 1011–1027, 1966.

[30] E. Bizzi, "Discharge patterns of single geniculate neurons during the rapid eye movements of sleep," *J. Neurophysiol.*, pp. 1087–1095, 1966.

[31] E. E. Fetz, "Operant conditioning of cortical unit activity," *Science*, pp. 955–958, 1969.

[32] D. M. Wolpert and J. R. Flanagan, "Motor learning," *Curr. Biol.*, pp. R467–472, 2010.

[33] J. Gordon, M. F. Gillardi, and C. Ghez, "Impairments of reaching movement in paitients without proprioception. I. Spatial errors," *J. Neurophysiol.*, pp. 347–360, 1995.

[34] D. Lee, N. L. Port, W. Kruse, and A. P. Georgopoulos, "Variability and correlated noise in the discharge of neurons in motor and parietal areas of the primate cortex," *J. Neurosci.*, pp. 1161–1170, 1998.

[35] E. Todorov and M. Jordan, "Optimal feedback control as a theory of motor coordination," *Nat. Neurosci.*, pp. 1226–1235, 2002.

[36] D. Marr, *Vision: A Computational Investigation into the Human Representation and Processing of Visual Information*. New York: Freeman, 1982.